Spreading of an Inkjet Droplet on a Solid Surface with a Controlled Contact Angle at Low Weber and Reynolds Numbers

Yangsoo Son, Chongyoup Kim,* Doo Ho Yang, and Dong June Ahn

Department of Chemical and Biological Engineering, Korea University, Anam-dong, Sungbuk-ku, Seoul 136-713, Korea

Received August 13, 2007. In Final Form: October 29, 2007

Even though the inkjet technology has been recognized as one of the most promising technologies for electronic and bio industries, the full understanding of the dynamics of an inkjet droplet at its operating conditions is still lacking. In this study, the normal impact of water droplets on solid substrates was investigated experimentally. The size of water droplets studied here was 46 μm and was much smaller than the most of the previous studies on drop impact. The Weber number (We) and Reynolds number (Re) were 0.05−2 and 10−100, respectively, and the Ohnesorge number was fixed at 0.017. The wettability of the solid substrate was varied by adsorbing a self-assembled monolayer of octadecyltrichlorosilane followed by the exposure to UV−ozone plasma. The impact scenarios for low We impacts were found to be qualitatively different from the high to moderate We impacts. Neither the development of a thin film and lamella under the traveling sphere nor the entrapment of small bubbles was observed. The dynamics of droplet impact at the conditions studied here is found to proceed under the combined influences of inertia, surface tension, and viscosity without being dominated by one specific mechanism. The maximum spreading factor (β), the ratio of the diameter of the wetted surface and the drop diameter before impact, was correlated well with the relationship ln $\beta = 0.090 \ln \mathrm{We}/(f_s - \cos\theta) + 0.151$ for three decades of $\mathrm{We}/(f_s - \cos\theta)$, where θ is the equilibrium contact angle, and f_s is the ratio between the surface areas contacting the air and the solid substrate. The result implies that the final shape of the droplet is determined by the surface phenomenon rather than fluid mechanical effects.

Introduction

During the past decade, the idea of inkjet printing has emerged as a class of technologies essential in many electronic and bio industries. Inkjet printing technology has been applied to three-dimensional shaping,[1−3] flat panel display,[4−9] printed circuit boards (PCBs),[10] semiconductor packaging,[2] and DNA chip and biosensors,[11−16] in addition to conventional printing, and is regarded as one of the most promising future technologies. In this research we will investigate the spreading processes of inkjet drops after the impact of a drop on solid surfaces. The impact of a liquid drop on a solid surface has been studied for almost 100 years since the pioneering work of Worthington[17] because of its relevance to many natural phenomena as well as industrial applications, and significant progress has been made in the understanding of the impact process theoretically, computationally, and experimentally. Recently Yarin[18] reviewed the drop impact dynamics comprehensively and delineated many interesting phenomena such as splashing, spreading, receding, bouncing, crown formation, and so on. Until now, most of the studies on drop impact have been focused on the Newtonian fluids. But there has been a growing interest on the drop impact of rheologically complex fluids reflecting many practical applications, including inkjet printing and spray painting. Zhang and Basaran,[19] Boger and his co-workers,[20−22] Bergeron et al.,[23] and Prunet-Foch and his co-workers[24,25] studied the impacts of surfactant solutions and polymer solutions experimentally and observed the effect of dynamic surface tension, elasticity, and shear thinning.

Schiaffino and Sonin[26] classified the drop impact into four different regimes according to Weber ($\mathrm{We} = \rho D U^2/\sigma$) and Ohnesorge ($\mathrm{Oh} = \eta/\sqrt{D\sigma\rho}$) numbers, where ρ is the density of the liquid, D is the diameter of the drop before impact, U is the impact velocity, σ is surface tension, and η is the viscosity of the liquid. In regime I, where $\mathrm{We} \gg 1$ and $\mathrm{Oh} \ll 1$, kinetic energy dominant motion prevails, and fluid behaves almost like an inviscid fluid; in regime II, where $\mathrm{We} \ll 1$ and $\mathrm{Oh} \ll 1$, capillarity drives the motion of inviscid fluids; in regime III,

* Corresponding author. E-mail: cykim@grtrkr.korea.ac.kr. Phone: +82-2-3290-3302.

(1) Derby, B.; Reis, N. *MRS Bull.* **2003**, *28*, 815−818.
(2) Mei, J. F.; Lovell, M. R.; Mickle, M. H. *IEEE Trans. Electron. Packag. Manuf.* **2005**, *28*, 265−273.
(3) Godlinski, D.; Morvan, S. *Mater. Sci. Forum* **2005**, *492−493*, 679−684.
(4) Kobayashi, H.; Kanbe, S.; Seki, S. *Synth. Met.* **2000**, *111*, 125−128.
(5) Shimoda, T.; Morii, K.; Seki, S. *MRS Bull.* **2003**, *28*, 821−827.
(6) de Gans, B.; Schubert, U. S. *Langmuir* **2004**, *20*, 7789−7793.
(7) Wang, J. Z.; Zheng, Z. H.; Li, H. W.; Huck, W. T. S.; Sirringhaus, H. *Nat. Mater.* **2004**, *3*, 171−196.
(8) Koo, H. S.; Chen, M.; Pan, P. C.; Chou, L. T.; Wu, F. M.; Chang, S. J.; Kawai, T. *Displays* **2006**, *27*, 124−129.
(9) Yoshioka, Y.; Jabbour, G. E. *Synth. Met.* **2006**, *156*, 779−783.
(10) Lopez, F. V.; Diez, A.; Odriozola, A. *Int. Polym. Process.* **2007**, *22*, 27−32.
(11) Li, C.; Wong, W. H. *Proc. Natl. Acad. Sci. U.S.A.* **2001**, *98*, 31−36.
(12) Heller, M. J. *Annu. Rev. Biomed. Eng.* **2002**, *4*, 129−153.
(13) Bietsch, A.; Hegner, M.; Lang, H. P.; Gerber, C. *Langmuir* **2004**, *20*, 5119−5122.
(14) Kumar, A.; Goel, G; Fehrenbach, E. *Eng. Life Sci.* **2005**, *5*, 215−222.
(15) Mukhopadhyay, R.; Lorentzen, M.; Kjems, J.; Besenbacher, F. *Langmuir* **2005**, *21*, 8400−8408.
(16) Wallace, D. B.; Taylor, D.; Antohe, B. V.; Achiriloaie, I.; Comparini, N.; Stewart R. M.; Sanghera, M. K. *Meas. Sci. Technol.* **2006**, *17*, 3102−3109.
(17) Worthington, A. M. *A Study of Splashes*; Longmans, Green: London, 1908.
(18) Yarin, A. L. *Annu. Rev. Fluid Mech.* **2006**, *38*, 159−192.
(19) Zhang, X.; Basaran. O. A. *J. Colloid Interface Sci.* **1997**, *187*, 166−178.
(20) Crooks, R. C.; Cooper-White, J. J.; Boger, D. V. *Chem. Eng. Sci.* **2001**, *56*, 5575−5592.
(21) Cooper-White, J. J.; Crooks, R. C.; Boger, D. V. *Colloids Surf., A: Phys. Eng. Aspects* **2002**, *210*, 105−123.
(22) Cooper-White, J. J.; Crooks, R. C.; Chockalingam, K.; Boger, D. V. *Ind. Eng. Chem. Res.* **2002**, *41*, 6443−6459.
(23) Bergeron, V.; Bonn, D.; Martin, J. Y.; Vovelle, L. *Nature* **2000**, *405*, 772−775.
(24) Rozhkov, A.; Prunet-Foch, B.; Vignes-Adler, M. *J. Non-Newtonian Fluid Mech.* **2006**, *134*, 44−55.
(25) Rozhkov, A.; Prunet-Foch, B.; Vignes-Adler, M. *Phys. Fluids* **2003**, *15*, 2006−2019.
(26) Schiaffino, S.; Sonin, A. A. *Phys. Fluids* **1997**, *9*, 3172−3187.

10.1021/la702504v CCC: $40.75
Published on Web 02/09/2008

where We $\ll$ 1 and Oh $\gg$ 1, capillary effect is dominant, and the viscosity of the fluid is important; finally, in regime IV, where We $\gg$ 1 and Oh $\gg$ 1, kinetic energy dominates the capillarity, and the viscous force is also important. Then they performed the drop impact experiments at low Weber numbers for various Ohnesorge numbers (regimes I and II) and gave the correlations for the velocity and time scale of spreading and the amplitude and time scale of oscillations that appeared after the spreading. They laid down the framework for understanding the impact phenomena at low We based on dimensional analyses and experiments. However, their work did not incorporate the wettability of a solid surface quantitatively. Rioboo et al.[27] demonstrated that the dimensionless groups We and Oh were less sensitive, and the wettability was the most important parameter in spreading dynamics. Many other studies have also reported the contact angle dependency of spreading dynamics. Recently, Ukiwe et al.[28] performed experiments on the spreading of water droplets with a diameter of 3.6 mm on self-assembled monolayers of alkanethiol. These monolayers can have systematically different hydrophilicity by varying the ratio of hydrophobic CH_3 and hydrophilic COOH terminal groups, and hence have different contact angles. Their results for a We of 59 and contact angles between 55.8° and 113° degrees showed that, within the early times of D/U of less than 1.4 ms, the spreading characteristics were almost equivalent for all surfaces. The spreading characteristic changed drastically, however, at the later stage of impact: When the contact angle is 55.8°, spreading is monotonic; when the contact angle is equal to or larger than 91°, recoil occurs in a substantial degree.

Until now, most of the drop spreading experiments have been performed for large Reynolds numbers, Re $= DU\rho/\eta = \sqrt{\text{We}}/\text{Oh}$ (100 − 2000) and Weber numbers (1−400) with drops 2−3 mm in diameter. At these conditions, the kinetic energy of the droplet overwhelms the surface energy, and hence the maximum spreading factor becomes large, where the maximum spreading factor is defined as the ratio of the diameter of a wetted surface on the wall and the initial diameter before impact, assuming a spherical shape. Also, there appeared to be capillary instability at the rim showing fingering and corona splash.[29−31] However, in most inkjet operations, the Reynolds number remains between 1 and 100 as a result of its small diameter even at high jetting velocities. When the drop is small, the final drop shape on a solid surface has to be a truncated sphere because of the strong surface tension effect. This constraint will make the difference in the deformation history of the drop, especially in the final stage of deformation. Therefore, we need to investigate the spreading dynamics with the same size droplet used in inkjet technology to understand the process properly. To study the spreading dynamics, a robust method of the formation of inkjet drops is essential. Recently, Dong et al.[32,33] studied the main stages of drop-on-demand (DOD) drop formation experimentally: ejection and pinch-off of liquid thread from the nozzle; contraction of the liquid thread and formation of primary and satellite drops; recombination of primary and satellite drops. Their experimental studies were performed by their state-of-the-art visualization technique[33] based on flash videography, assuming that the process is totally reproducible after the initial unsteadiness which is the so-called "first-drop problem." As far as the authors are aware of, the DOD drop formation is still not an established technique, and the optimum operating condition is not available at a given set of an inkjet head and liquid. By adopting suitably devised pressure waveforms to the piezoelectric head, one may control the drop size beyond the normally available drop size for a given nozzle size. Chen and Basaran[34] were able to reduce the drop radius to approximately 1/3 of the nozzle radius experimentally and showed the mechanism of the formation of such a small drop by a numerical method. Their work can be applicable to the drop formation of a suspension of relatively large particles while using a large-radius nozzle with reduced clogging problems. Van Dam and Le Clerc[35] investigated the spreading dynamics with inkjet droplets 36−85 μm in diameter. They explored the relatively large We (0.5−100) and found that the initial impact was followed by a rapid radial flow, and an oscillatory motion set in after a moderate rebound. Dong et al.[33] also considered the impact of an inkjet drop on two different surfaces with widely different contact angles. However, their study was limited to the case of We = 10.7, and no systematic study was performed for various solid surfaces. Even though their works revealed some important information on the inkjet drop spreading, the range of We was restricted to large cases, and therefore the full understanding of inkjet droplet dynamics is far from being complete. Another issue in drop impact is the entrapment of a bubble at the bottom of the drop even at a moderate condition of impact.[35,36] Since the presence of a bubble can deteriorate the inkjet coating quality, it should be avoided. On the other hand, the jetting speed should not be too slow to have a higher printing or coating speed as well as the proper ballistic trajectory. Therefore, we need to designate a proper operating window for a fast, yet stable inkjet operation.

When We and Re are close to 1, the kinetic energy of the droplet is comparable to the surface energy, and the viscous force cannot be neglected. Therefore, during the spreading, kinetic and surface energies compete with each other under the influence of the viscous force. As far as the authors are aware of, until now, no study has been reported on the droplet spreading in this regime. Therefore, the objective of this paper is to understand the low Weber and Reynolds number deposition of liquid drops on surfaces with controlled contact angle to represent the inkjet droplet impact, which has not been explored by the previous inkjet studies by Dong et al.[33] and van Dam and Le Clerc.[35] We have explored the impact of an inkjet drop when the surface energy is larger than or comparable to the kinetic energy. Specifically, the Weber number has been confined to 0.05−2 so that the surface energy is 1−10 times the kinetic energy. In this regime, we have been able to avoid splashes and bubble formation. Since the droplet size is fixed at 46 μm, we changed the impact velocity to change the We. We have found that the magnitude of the maximum spreading was not correlated well with Reynolds or Weber numbers, as in the case of large drops with large kinetic energy. In this range of We, the surface condition of the substrate should be very important in the impact process. Therefore, we have examined the role of the work of adhesion and have found that the magnitude of maximum spreading is a function of the modified Weber number only based on the surface energy at the end of the impact rather than the Weber number based on the liquid−vapor surface tension.

(27) Rioboo, R.; Marengo, M.; Tropea, C. *Exp. Fluids* **2002**, *33*, 112−124.
(28) Ukiwe, C.; Mansouri, A.; Kwok, D. Y. *J. Colloid Interface Sci.* **2005**, *285*, 760−768.
(29) Xu, L; Zhang, W. W.; Nagel, S. R. *Phys. Rev. Lett.* **2005**, 184505.
(30) Lee, H. J.; Kim, H. Y. *Phys. Fluids* **2004**, *16*, 3715−3719.
(31) Rioboo, R.; Bauthhier, C.; Conti, J.; Voue, M.; De Coninck, J. *Exp. Fluids* **2003**, *35*, 648−652.
(32) Dong, H. M.; Carr, W. W.; Morris, J. F. *Phys. Fluids* **2006**, *18*, 072102.
(33) Dong, H. M.; Carr, W. W.; Morris, J. F. *Rev. Sci. Instrum.* **2006**, *77*, 085101.
(34) Chen, A. U.; Basaran, O. A. *Phys. Fluids* **2002**, *14*, L1−L4.
(35) van Dam, D. B.; Le Clerc, C. *Phys. Fluids* **2004**, *16*, 3403−3414.
(36) Sikalo, S.; Wilhelm, H. D.; Roisman, I. V.; Jalirilic, S.; Tropea, C. *Phys. Fluids* **2005**, *17*, 062103.

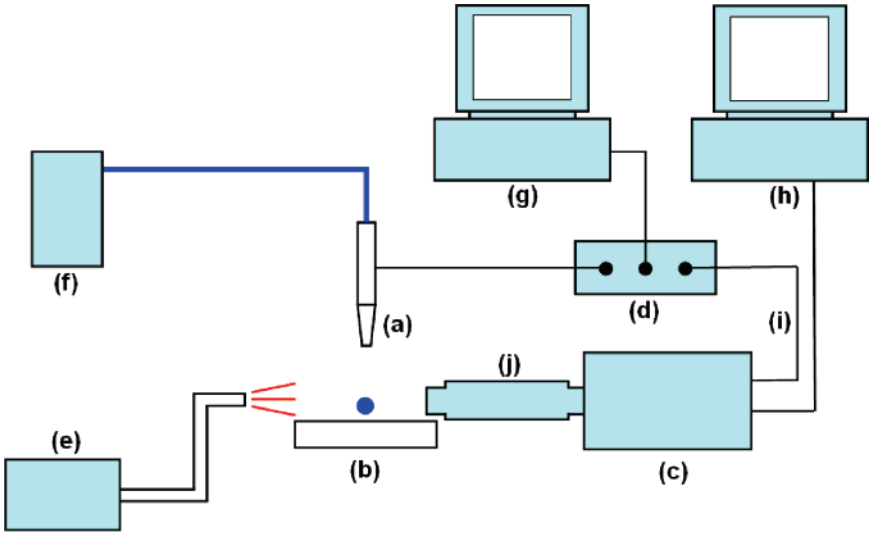

Figure 1. Schematic diagram of the experimental setup: (a) inkjet nozzle; (b) solid substrate with controlled contact angle; (c) high-speed camera; (d) jetting driver; (e) illumination source; (f) pneumatic system; (g) jetting control computer; (h) image processing computer; (i) triggering; (j) objective lens.

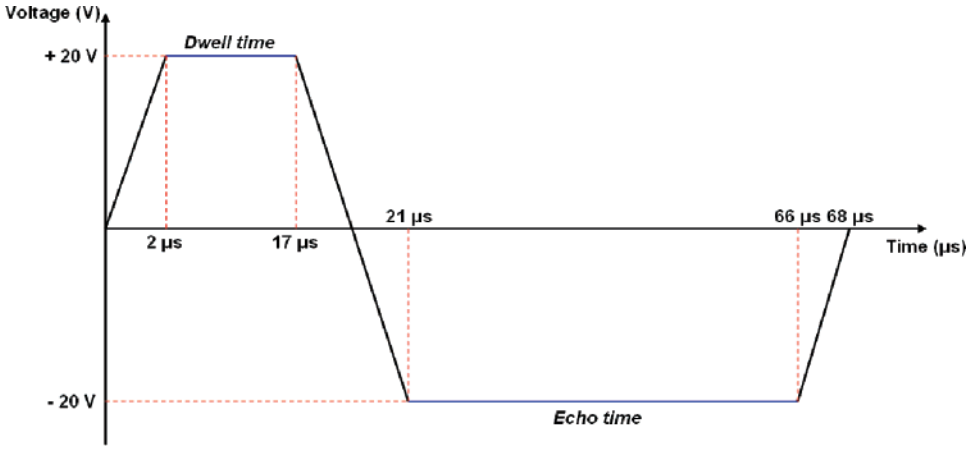

Figure 2. A typical voltage wave form used in the experiment.

Experimental Method

To investigate the impact dynamics of inkjet drops, we set up an inkjet system as in Figure 1. The system consists of an inkjet nozzle, a jetting driver (pulse generating system), a high-speed camera, and an illumination source. Microdrops generated from the inkjet nozzle were impinged on glass surfaces. The wettability of glass surface was controlled by adsorbing a self-assembled monolayer of octadecyltrichlorosilane (OTS) and a subsequent treatment with UV−ozone plasma. Double-distilled water was used as the liquid.

Inkjet System and Imaging. The inkjet nozzle was a piezo-type nozzle purchased from MicroFab Co. (Model # MJ-AT). The nozzle diameter was 50 μm. The distance between the nozzle tip and glass surface was set at 0.4 or 0.8 mm. In the piezo-type inkjet system, a train of voltage pulse is generated and transferred to the nozzle where the piezo element is contracted and expanded according to the pulse to generate a liquid thread. As the thread travels in the air it becomes a spherical droplet under the action of surface tension. In the inkjet system, it is very important to choose a proper operating condition because, depending on the operating conditions, satellite drops can be followed by the main drop. To avoid such a problem, a well-conditioned acoustic wave has to be generated in the nozzle by choosing a proper pressure wave to the piezo element. In this research, we used the wave form shown in Figure 2: in the figure, the rise time and decay time in the voltage pulse to the nozzle were fixed at 2 μs, the dwell time was set to be 45−60 μs and 2−3 times longer than the echo time, and the ranges of the dwell and echo voltages were set at +15 to +30 V and −15 to −30 V, respectively. Under the set of these conditions, inkjet drops of 46 μm were generated without generating satellite droplets behind the main droplet. The temperature of the drop was 309 K. At this condition, the Ohnesorge number of the droplet was 0.017. The high-speed camera (Redlake, MotionPro X-4) was triggered by the jetting driver as a droplet was ejected from the inkjet nozzle. The camera was equipped with a microscopic objective lens (Mitutiyo, M plan Apo 20x) with the magnification of 20×. As the illumination source, a back lighting system (Stocker Yale, # 21AC, 180W) was installed.

The charge-coupled device (CCD) camera can take 100 000 frames per second, and some of the pictures were taken with this mode. But when this fast mode was used, the number of pixels per frame has to be small (512 × 20 pixels), hence the quality of the picture is not good. Also, since the inertial and capillary time scales of the process are approximately the same as the interval between two successive frames, it is not possible to capture the drop dynamics. So we also used a modified method called "flash videography" to obtain a picture with better resolution by varying the time delay between the drop impingement and triggering of the shutter of the CCD. To reduce the number of experiments, we took pictures every 33 μs for each delayed experiment and arranged the pictures according to the elapsed time. The delay times were 1/4, 1/2, and 3/4 of 33 μs. To obtain a series of pictures at each condition, we performed at least five sets of experiments and then checked the reproducibility. The exposure time was 5 μs, and each frame had 512 × 80 pixels. The pixel size was 0.96 μm. For the state-of-the-art application of the flash videography, the reader can refer to Dong et al.'s[33] exquisite

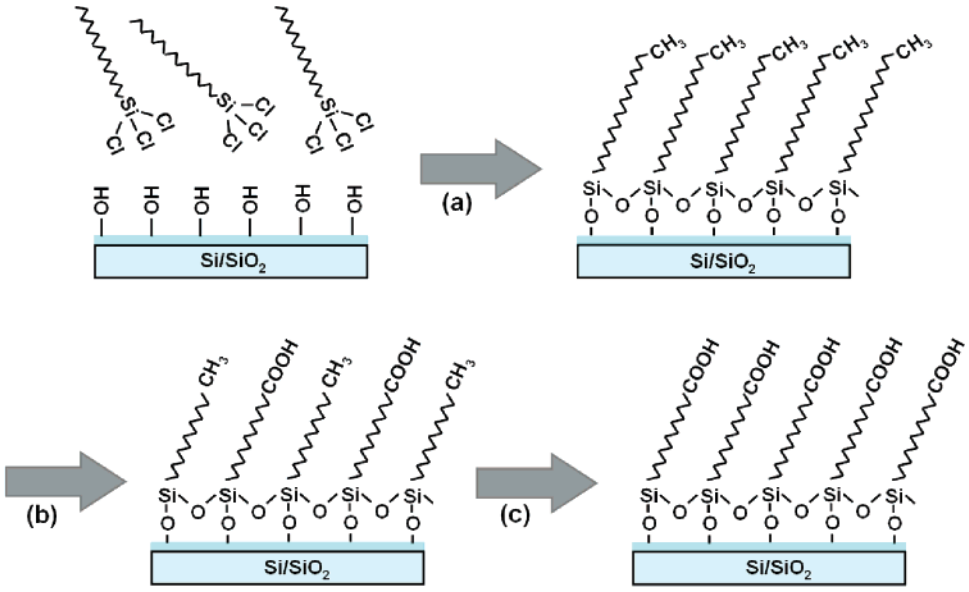

Figure 3. Procedure for controlling the contact angle of a glass surface. A hydrophobic self-assembled monolayer is adsorbed and then treated with UV−ozone to control the hydrophilicity by varying the exposure time: (a) adsorption and reorientation of SAMs; (b) UV−ozone plasma treatment for partial oxidation; (c) extended UV−ozone treatment to increase the wettability.

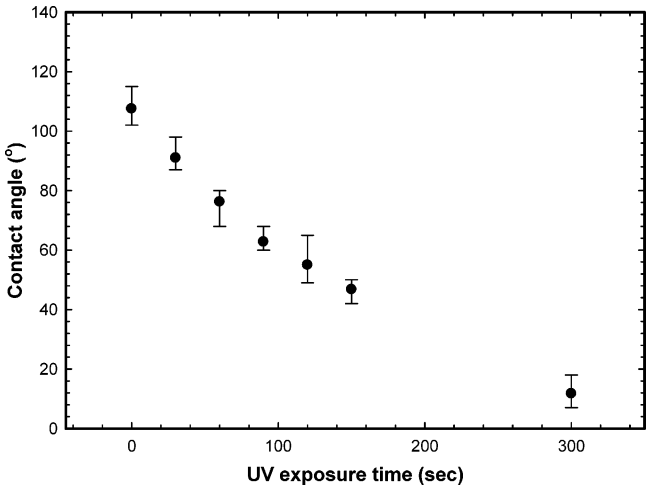

Figure 4. Contact angle changes with the variation of the exposure time to UV−ozone plasma. As the exposure time increases, the wettability increases.

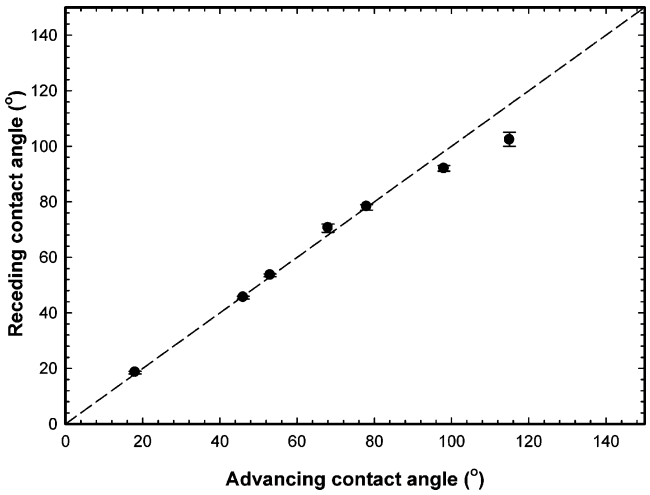

Figure 5. Receding vs advancing contact angle values. In this case, the two values are almost the same. The diagonal line is for guiding the eyes.

implementation for the study of the formation of an inkjet drop. This method is based on the assumption that each impingement and drop deformation is reproducible in time and position. However, in the case of low Weber numbers, it has been found that the result is not always reproducible, as compared to the perfect reproducibility after the first drop problem in Dong et al.'s studies.[32,33] This problem was also reported by van Dam and Le Clerc.[35] Only 7 out of 10 experiments appear to follow the same process at one condition. Therefore, we chose the seven experiments to represent the result at that condition. The reproducibility of impact dynamics was even poorer as a result of its highly sensitive nature to surface conditions. This prohibits us from using the standard flash videography. To observe the spreading dynamics of a drop by a single experiment, one may have to use an ultrafast camera that can capture as many as 10^8 frames/s such as that used by Basaran's group[37,38] in the study of thread pinch-off and satellite drop formation.

Control of Contact Angle by SAMs. Glass substrates with controlled wettability were prepared by using the scheme shown in Figure 3 following the method given in the literature.[39−41] First, a glass slide is made hydrophilic by a UV−ozone treatment. Then the surface was transformed to hydrophobic by adsorbing a self-assembled monolayer of OTS. Unadsorbed OTS was eliminated by repeated washing with distilled water and nitrogen purging. OTS was rearranged by backing glasses, and then physisorbed OTS was eliminated by an ultrasonic treatment. Finally, the glass was washed with distilled water to finally obtain the hydrophobic surface. The contact angle of each hydrophobic surface was measured to confirm its hydrophobicity. Controlled hydrophilicity was obtained by treating the hydrophobic surface with UV−ozone plasma by oxidizing CH_3 at the end of OTS to COOH. Depending on the exposure time to UV−ozone, the hydrophilicity varied.

In Figure 4, the contact angle (θ) values measured with an advancing mode (sessile drop method) are plotted against the exposure time to UV−ozone. As treatment time increases, the surface becomes more hydrophilic. We also measured the contact angle in a receding

(37) Notz, P. K.; Chen, A. U.; Basaran, O. A. *Phys. Fluids* **2001**, *13*, 549−552.
(38) Chen, A. U.; Notz, P. K.; Basaran, O. A. *Phys. Rev. Lett.* **2002**, *88*, 174501.
(39) Ulman, A. An *Introduction to Ultrathin Organic Film from Langmuir−Blodgett to Self-Assembly*; Academic Press: New York, 1991; pp 237−304.
(40) Yasseri, A. A.; Sharma, S.; Kamins, T. I. *Appl. Phys. Lett.* **2006**, *89*, Art. No. 153121.
(41) Xue, C. Y.; Yang, K. L. *Langmuir* **2007**, *23*, 5831−5835.

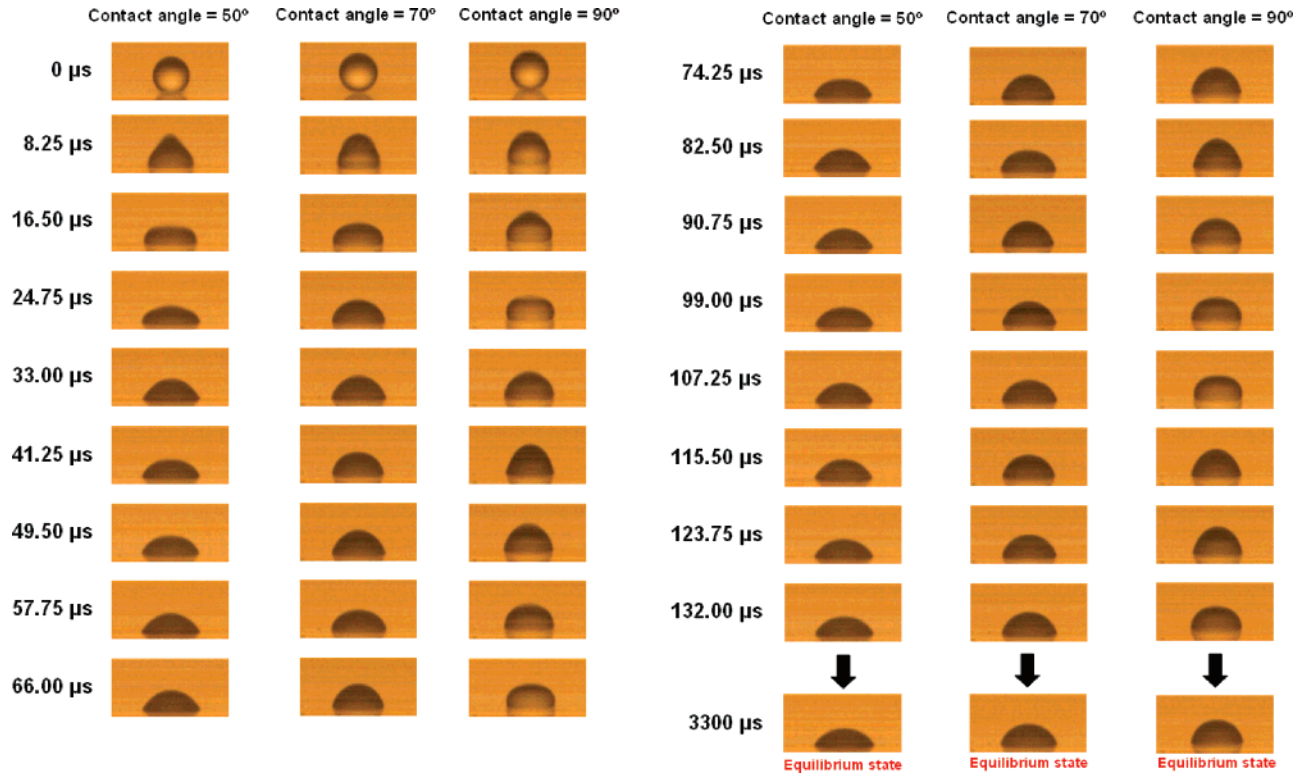

Figure 6. Drop impact dynamics on three different surfaces with contact angles of 50, 70, and 90° when We = 1.23 and Oh = 0.017. Depending on the wettability of surface, the drop deformation after the impact changes significantly. However, no lamella is formed. There are oscillations along the vertical and horizontal directions.

mode (pendant drop method) and compared the values obtained by the two methods, as shown in Figure 5. Except in the case of a hydrophobic surface, the two methods give almost the same value.

Results and Discussion

In this research, We was varied between 0.05 and 2. Therefore, our impact regime is between regimes I and II of Shiaffino and Sonin's classification,[26] and hence neither the inertial nor capillary effect is dominant. Bond number ($Bo = \rho g D^2/\sigma$) is 2.8×10^{-4} and is so small that the gravitational effects are entirely negligible during impact and spreading, and the final shape of the drop takes the truncated spherical form. As pointed out in the Introduction, there has been no report on drop impact for this range of We and Oh. We describe the drop impact scenario in the following.

Droplet Spreading Scenario. Figure 6 shows the series of images for the impact and spreading of water drops on surfaces with different hydrophilic nature. The three sets of images in the figure show that, depending on the hydrophilic nature of the surface, the drop deformation history is not quite similar except for the initial phase of impact: Upon hitting the surface, the droplet deforms until it has the shape of a disc with rounded sides regardless of hydrophilicity (at 16.5 μs for $\theta = 50°$ and 70°; 24.75 μs for $\theta = 90°$). However, the subsequent changes in droplet shape are different for different substrates: In the case of a wetted surface ($\theta = 50°$), the fluid near the substrate spreads monotonically, and the overall drop shape keeps a truncated-sphere form. However, on a hydrophobic surface ($\theta = 90°$), the upper part of the drop recedes until it takes the shape of a half of a prolate spheroid (at 41.25 μs). It then oscillates afterward until viscous dissipation consumes the remaining kinetic energy. At the end of the inertial spreading, the spreading factors for two cases are 1.57 and 1.28, respectively. On the hydrophobic surface, the drop recedes about 8% from the maximum spreading when it has a disc shape. The maximum value of the spreading factor for $\theta = 90°$ in this research is much smaller than the value reported by Ukiwe et al.[28] where they reported that the maximum diameter is approximately 3.1 times larger than the initial drop diameter when We is approximately 50 at virtually the same value of contact angle ($\theta = 91°$). We also note that no lamella is formed or ejected at the initial stage, and no capillary wave or fingering is observed at the later stage. Also no air bubble was entrapped as Pasandideh-Fard et al.,[42] Sikalo et al.,[36] and Van Dam and Le Clerc[35] observed, meaning that the impact regime is different from theirs.

When $\theta = 10°$ and 110° (See Figure 7), the drop deformation is not similar to the previous cases, even at the initial stage. When $\theta = 10°$, the drop does not take the shape of a disc with rounded sides during spreading because the capillary spreading at the contact line is fast enough not to take such a stage. But there is still a weak, vertical oscillation due to non-negligible inertia. The oscillation characteristic will be discussed in the next section. When $\theta = 110°$, the drop does not take the shape of a disc with rounded sides either. It is observed that the contact line is almost pinned after the initial stage of impact, and only the upper part of the drop oscillates. This means that the shear flow inside the drop is weak.

In Figure 8, we show the shapes of droplets on surfaces with different contact angles at the end of the inertial spreading. When the Weber number is large, it has been reported that, regardless of wettability, the dynamic contact angle remains at the same value of about 130° in the time interval $0.1 < tU/D < 2$ (Sikalo et al.[36]). It was also predicted by a theoretical model by Roisman et al.[43] However, when the Weber number is between 0.05 and

(42) Pasandideh-Fard, M.; Quio, Y. M.; Chandra, S.; Mostaghimi, J. *Phys. Fluids* **1996**, *8*, 650−659.
(43) Roisman, I. V.; Rioboo, R.; Tropea, C. *Proc. R. Soc. London* **2002**, *458*, 1411−1430.

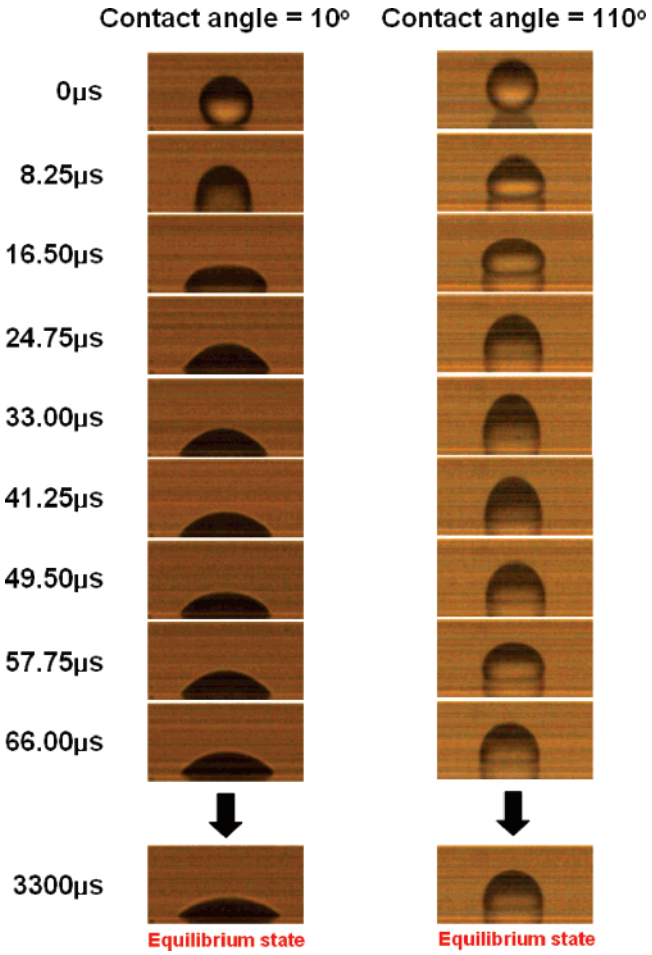

Figure 7. Drop impact dynamics on two different surfaces with contact angles of 10 and 110° at the same impact condition as in Figure 6. The drop deformation after the impact differs significantly. The drops take spherical shapes at the equilibrium state regardless of contact angle.

2, the dynamic contact angle shows a different value, even at the initial phase of deformation, reflecting the wettability of substrate.

Oscillation of the Drop. Since the first paper on the oscillation of free drops by Rayleigh,[44] this topic has been extensively studied both theoretically and experimentally. The oscillation of pendant or sessile drops was systematically studied by Strani and Sabetta[45] for inviscid fluid, and Basaran and DePaoli[46] and Wilkes and Basaran[47] for free and forced oscillations of viscous fluids, respectively. Next we describe the oscillation characteristics of an inkjet drop when the Reynolds number is based on the capillary velocity $\sqrt{\rho D\sigma/2}/\eta = 41$.

In our regime, the capillary velocity $\sqrt{2\sigma/\rho D} \approx 1.8$ m s^{-1} is comparable to the original impact velocity $U \cong 1$ m s^{-1}, hence the top center of the drop does not show a large curvature as reported in the case of small We and small Oh.[26,27,35] Since the large curvature at the top induces a strong downward motion due to strong surface tension force, the drop takes a torus shape, and the strong vertical oscillations will ensue. Since there is no such large curvature in the present case, the oscillation mode is different from the inviscid, capillary-driven mode. In the other case of large We, the transient maximum spreading is large to have a small contact angle on even a hydrophobic surface. This will induce a strong receding motion, and, in the extreme case, the rebound of the drop occurs.[28] As shown in Figures 9, the oscillation mode is found to be a small amplitude motion with a varying degree of spreading diameter. The height, contact line and contact angle oscillate with an oscillation frequency close to the surface tension-driven oscillation ($\tau = \sqrt{\rho D^3/8\sigma} = 13$ μs). The oscillations are damped within a few cycles, reflecting that the viscous effect cannot be neglected. It is noteworthy that the result of $\theta = 10°$ was closely predicted by Basaran and DePaoli[46] for a thin drop with a pinned contact line when Re = 40 and Bo = 0 (Figure 7 of the present study and Figure 9 of their paper) despite a slight difference in the contact line motion. When $\theta = 110°$, the agreement is not as good as the case of $\theta = 10$. However, the qualitative nature of oscillation appears well matched to each other (Figure 7 of the present study and Figure 8 of Basaran and DePaoli[46]). The major difference between the present experiment and Basaran and DePaoli's numerical results is the damping rate. The damping rate of the present study is much faster, probably because the contact line is moving, while, in Basaran and DePaoli's case, the contact line is pinned, hence the viscous dissipation is less. When compared with the numerical results for forced oscillation by Wilkes and Basaran,[47] the oscillation characteristics are not the same, and no concave surface is observed at the top of the drop experimentally. On the basis of Hoffman−Tanner−Voinov law,[48,49] Schiaffino and Sonin[26] estimated that the Ohnesorge number at the boundary of the inertial regime and viscous regime could be as low as 0.01. In the present research, we observed the roles of both the inertial and viscous effects in oscillations, regardless of contact angle. There is a delicate balance of inertia, surface tension, and viscous forces in this regime.

Equilibrium Shape. In Figure 10, we have plotted the equilibrium contact angle after drop impacts for differing static contact angles when We = 1.23 (from the experiments shown in Figures 6 and 7). The contact angles attained by the droplet on substrates are not the same as the equilibrium contact angle showing contact angle hysteresis. When the static contact angle is small, the equilibrium contact angle is larger than the static contact angle. This means that the contact line movement dissipates a significant amount of the kinetic energy. In the case of hydrophobic surface, the equilibrium contact angle is comparable or even smaller than the static contact angle. This appears to be caused by the receding motion concomitant with the oscillatory motion on non-hydrophilic surfaces.

In Figure 11, we have plotted the maximum spreading β against the contact angle of a solid substrate. The magnitude of the maximum spreading factor is an important concept, not just because it is a quantitative measure in theoretical analyses of the impact process. It determines pixel size in inkjet printing or

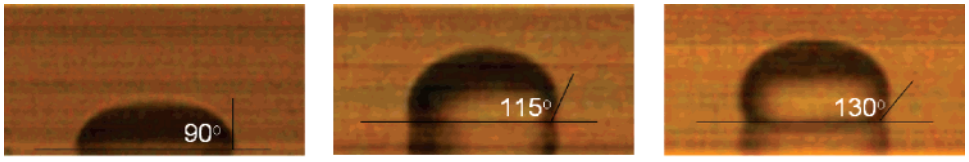

Figure 8. The contact angle values when the drop takes the maximum diameter of the wetted area (the maximum spreading condition). The contact angle values are not the same and increase with the static contact angle.

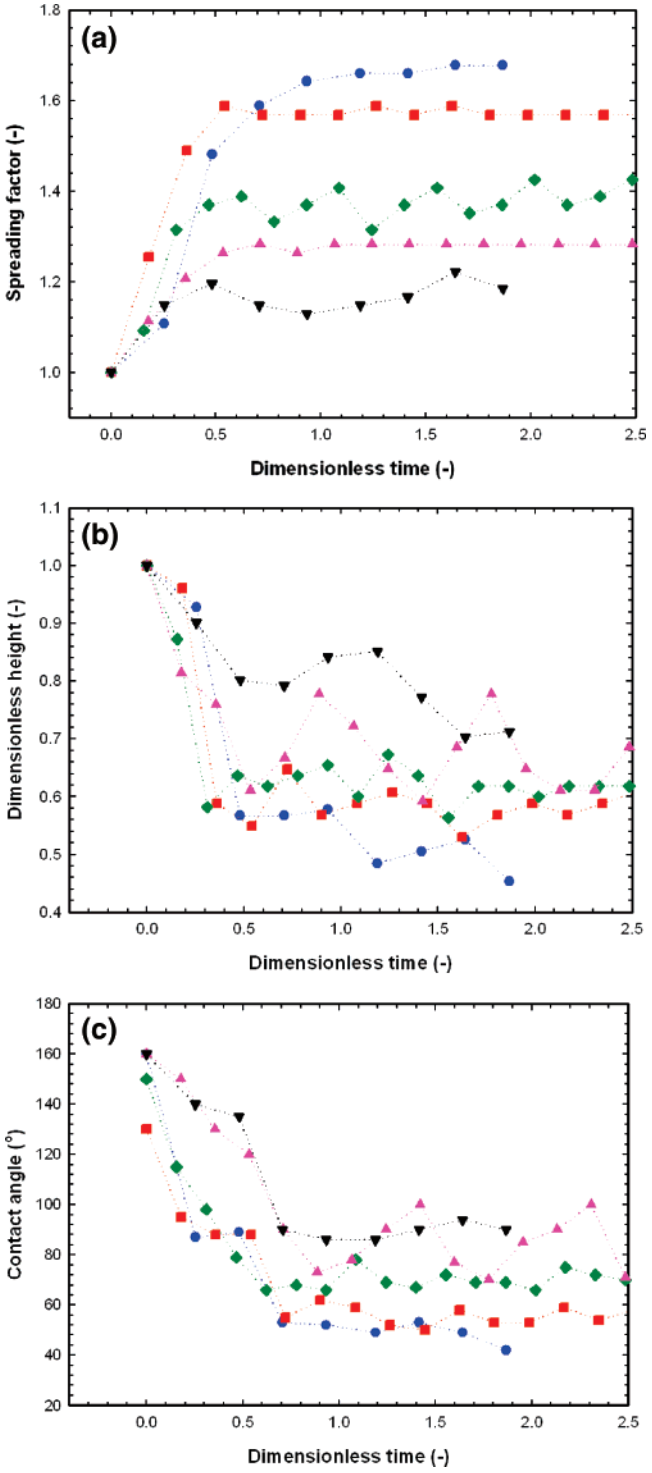

Figure 9. Changes of the maximum spreading (a), drop height (b), and contact angle (c) with dimensionless time. The dimensionless time is made from the inertial time (tU/D). After the initially fast changes, the drops oscillate with a period comparable to the time scale. The diameter and height take the equilibrium values after several oscillations. (●: contact angle = 10°; ■: contact angle = 50°; ♦: contact angle = 70°; ▲: contact angle = 90°; ▼: contact angle = 110°).

coating process since the contact line does not recede after it reaches the maximum diameter in the impact of particle-laden fluid, which is called "contact line pinning". Schiaffino and

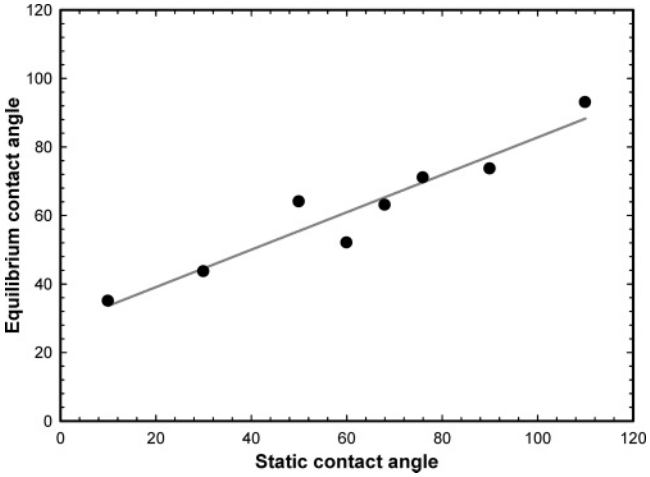

Figure 10. The equilibrium contact angle after the impact vs the static contact angle. When the static contact angle is small, the contact line stops before the contact angle reaches the static value. This is caused by the viscous dissipation during spreading. For large static contact angles, the equilibrium angle is smaller than the static angle as a result of the receding motion during oscillation.

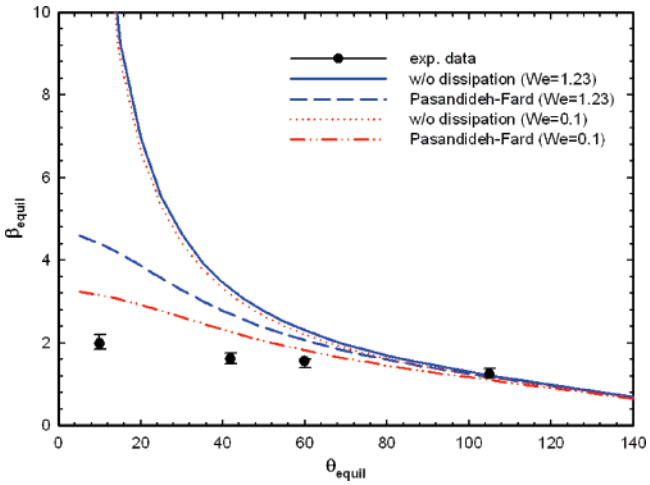

Figure 11. Measured maximum spreading values compared with the model predictions. Experimental values were obtained for various We values between 0.1 and 1.23. The deviations become large for small contact angles. This difference appears to be the result of the large viscous dissipation near the contact line.

Sonin[26] obtained that the maximum spreading factor is 2.4, and it approached exponentially with the capillary time scale, regardless of the type of materials (water on glass, water on ice, mercury) in region II (We, Oh ≪ 1). In our case, the value is below 2, and the approach to the equilibrium values is not monotonic as discussed above. It again implies that the regime we are considering not be matched to the scheme suggested by Schiaffino and Sonin.[26]

There have been numerous attempts to predict the maximum spreading by hydrodynamic modeling.[28,36,42,43,50,51] In most of the theoretical analyses, a cylindrical shape was assumed to determine the surface energy when the Weber number is much larger than 1. However, in the present case, this assumption is no longer valid, as seen in Figures 6 and 7. Our regime does not belong to the highly viscous cases with high capillarity either.

(44) Rayleigh, J. W. S. *Proc. R. Soc. London, Ser. A* **1879**, *29*, 71.
(45) Strani, M.; Sabetta, F. *J. Fluid Mech.* **1988**, *189*, 397−421.
(46) Basaran, O. A.; DePaoli, D. W. *Phys. Fluids* **1994**, *6*, 2923−2943.
(47) Wilkes, E. D.; Basaran, O. A. *Phys. Fluids* **1997**, *9*, 1512−1528.
(48) Hocking, L. M. *Phys. Fluids* **1995**, *7*, 2950−2955.
(49) Hoffman, R. L. *J. Colloid Interface Sci.* **1975**, *50*, 228−241.
(50) Chandra, S.; Avedesian, C. T. *Proc. R. Soc. London* **1992**, *432*, 13−41.
(51) Attané, P.; Girard, F.; Morin, V. *Phys. Fluids* **2007**, *19*, 012101.

Therefore, a direct comparison with the existing models could be meaningless. Nevertheless, in Figure 11, we compare the experimental data with three different models, all of which are based on the energy balance approach: the sum of the initial kinetic and surface energies is the same as the sum of the surface energy at the end of spreading and the viscous dissipation during spreading. As written below, we modified Pasandideh-Fard et al.'s model[42] by inserting the exact value of the surface area contacting the air. Therefore, the value of 1, which corresponds to the surface area of a circle, is replaced by f_s, which corresponds to the surface area of the truncated sphere:

$$\beta = \sqrt{\frac{\mathrm{We} + 12}{3(f_s - \cos\theta) + 4\mathrm{We}/\sqrt{\mathrm{Re}}}} \quad (1)$$

where $f_s = 1 + [1 - \cos\theta/\cos(90 - \theta)]^2$. When there is no viscous dissipation, this equation becomes[35]

$$\beta = \sqrt{\frac{\mathrm{We} + 12}{3(f_s - \cos\theta)}} \quad (2)$$

We also consider Ukiwe et al.'s modification[28] of Pasandideh-Fard et al.'s model[42] by correcting the surface energy term at the maximum speed.

$$(\mathrm{We} + 12)\beta = 8 + \beta^3\left[3(1 - \cos\theta) + 4\frac{\mathrm{We}}{\sqrt{\mathrm{Re}}}\right] \quad (3)$$

All these energy balance models give the higher values in β and the deviation becomes larger as θ decreases, as shown in Figure 11. This implies that the dissipation near the contact line cannot be neglected in the energy balance, especially when the contact angle is small and therefore a relatively long movement of contact line is required compared with the case of large contact angles.

From the fact that the kinetic energy, surface energy, and viscous dissipation are all related in the impact process, and none of these is dominating the dynamics, the setup of a simple dynamic model as reported in the literature for asymptotic cases appears to be impossible. Numerical solutions may predict the dynamics accurately, but numerical modeling is beyond the scope of the present article. Therefore, to predict the maximum spreading, we focused on the equilibrium shape without considering the dynamic process. In view of the fact that the surface energy between the liquid and solid is important, we modified the Weber number by replacing the surface tension between liquid and air by the surface energy of the droplet at equilibrium after the impact as follows:

$$\mathrm{We}' = \frac{\mathrm{We}}{(f_s - \cos\theta)} \quad (4)$$

In Figure 12, we have plotted the spreading factor against the modified Weber number. The figure shows that the spreading factor is a weakly varying function of the modified spreading factor We′ only for three decades and has the following relationship:

$$\ln\beta = 0.090 \ln \mathrm{We}' + 0.151 \quad (5)$$

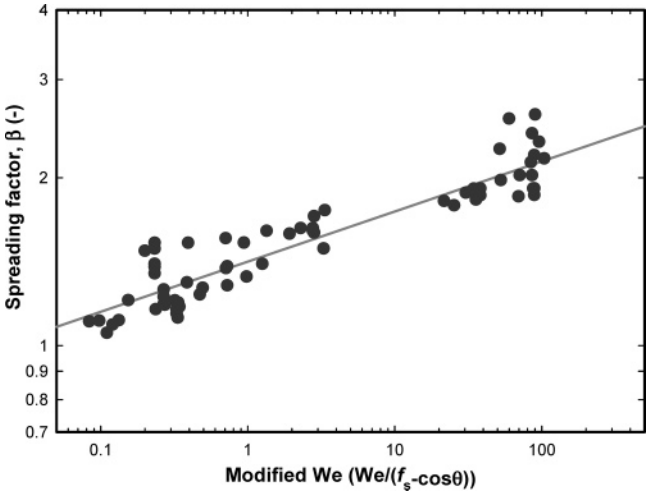

Figure 12. Spreading factor vs the modified Weber number based on the impacts on different surfaces with different velocities. The spreading factor (β) is well correlated with the relationship $\ln\beta = 0.090 \ln \mathrm{We}' + 0.151$, with $r^2 = 0.846$.

From this relationship, one may proceed to obtain a more precise model for the impact dynamics when the inertia, surface tension, and viscosity are all important. The good correlation implies that the final shape of droplet be determined primarily by the surface phenomena rather than fluid mechanical effects, regardless of wettability for We and Oh regimes considered here.

Conclusion

In this research we explored the impact of an inkjet droplet on solid substrates with controlled wettability when Weber numbers have an order of 1 or lower (0.05−2) and the Reynolds number remains below 100. The Ohnesorge number was 0.017. The droplet diameter studied here is 2 orders of magnitude smaller than most of the studies reported previously. The impact scenarios for low We impacts were found to be qualitatively different from the high We impacts. We did not observe the development of a thin film or lamella under the traveling sphere. Therefore, the existing models such as one-dimensional cylindrical models based on such flows are not suited for the impact regime considered here. In this case, the impact is weak enough not to form a lamellar or thin film, but strong enough to induce oscillations along the axial direction (and radial direction too) and to retard the fast contact line motion. The droplet impacts at the conditions studied here are found to proceed under the combined influences of inertia, surface tension, and viscosity. In determining the maximum spreading factor, the energy balance models in the literature are not suited for impacts with the range of parameters treated here. Considering the importance of the surface energy after the impact, a modified We number was defined by dividing We by ($f_s - \cos\theta$). It was found that the maximum spreading factor was a weakly varying function of the modified Weber number only for three decades, proving the importance of the surface phenomena over the fluid mechanical effects.

Acknowledgment. This work was supported by Grant No. R01-2006-000-10267-0 from the Basic Research Program of the Korea Science & Engineering Foundation.

LA702504V